Extracting glacier calving fronts by deep learning: the benefit of multi-spectral, topographic and textural input features

Erik Loebel, Mirko Scheinert, Martin Horwath, Konrad Heidler, *Student Member, IEEE,* Julia Christmann, Long Duc Phan, Angelika Humbert, and Xiao Xiang Zhu, *Fellow, IEEE,*

Abstract—An accurate parameterization of glacier calving is essential for understanding glacier dynamics and constraining ice-sheet models. The increasing availability and quality of remote sensing imagery opens the prospect of a continuous and precise mapping of relevant parameters such as calving front locations. However, it also calls for automated and scalable analysis strategies. Deep neural networks provide powerful tools for processing large quantities of remote sensing data. In this contribution, we assess the benefit of diverse input data for calving front extraction. In particular, we focus on Landsat-8 imagery supplementing single band inputs with multi-spectral data, topography and textural information. We assess the benefit of these three datasets using a *dropped-variable* approach. The associated reference dataset comprises 728 manually delineated calving front positions of 23 Greenland and 2 Antarctic outlet glaciers from 2013 to 2021. Resulting feature importances emphasize both the potential integrating additional input information as well as the significance of their thoughtful selection. We advocate utilizing multi-spectral features as their integration leads generally to more accurate predictions compared to conventional single band inputs. This is especially prevalent for challenging ice-melange and illumination conditions. In contrast, the application of both textural and topographic inputs cannot be recommended without reservation since they may lead to model overfitting. The results of this assessment are not only relevant for advancing automated calving front extraction but also for a wider range of glaciology-related land surface classification tasks using deep neural networks.

Index Terms—Greenland, glacier front, optical data, deep learning, feature importance

E. Loebel, M. Scheinert and M. Horwath are with the Technische Universität Dresden, Institut für Planetare Geodäsie, 01069 Dresden, Germany. (e-mail: erik.loebel@tu-dresden.de)

K. Heidler and X. Zhu are with the Remote Sensing Technology Institute, German Aerospace Center, 82234 Wessling, Germany and also with the Data Science in Earth Observation, Technical University of Munich, 80333 Munich, Germany.

J. Christmann is with the Alfred-Wegener-Institut Helmholtz Zentrum für Polar- und Meeresforschung, Sektion Glaziologie, 27568 Bremerhaven, Germany and also with the Technische Universität Kaiserslautern, Lehrstuhl für Technische Mechanik, 67653 Kaiserslautern, Germany.

L. Phan is with the Alfred-Wegener-Institut Helmholtz Zentrum für Polar- und Meeresforschung, Sektion Glaziologie, 27568 Bremerhaven, Germany.

A. Humbert is with the Alfred-Wegener-Institut Helmholtz Zentrum für Polar- und Meeresforschung, Sektion Glaziologie, 27568 Bremerhaven, Germany and also with the Universität Bremen, Fachbereich Geowissenschaften, 28359 Bremen, Germany.

I. INTRODUCTION

CALVING of marine terminating outlet glaciers results in seasonal and interannual changes of their frontal positions. These calving front variations are both, triggered by changes in the glacier dynamics, but also affect the dynamics of tidewater glaciers [1–3]. The accurate detection of calving rates is crucial for investigating the physical mechanism and controlling factors [4–8]. Moreover, accurately representing calving front dynamics in models is an essential part of constraining glacial evolution [9] and can improve simulations of mass loss and projections of future sea-level contributions [10–14]. Consequently, temporally and spatially comprehensive calving front datasets are essential for a better understanding and modelling of marine terminating glaciers.

The increasing availability and quality of both optical as well as radar satellite imagery enable us to realize a continuous mapping of calving front locations. However, most current calving front datasets [15–21] are based on manual delineation which is laborious and infeasible considering the immense data volume. Therefore, calving front records are often limited in temporal resolution making seasonal analyses difficult. The huge amount of data accentuates the necessity for automated and scalable delineation strategies. Driven by this issue various empirical feature extraction algorithms have been developed in the last decades pursuing robust automated calving front extraction [22–27]. However, most of these methods require case specific modifications and are not tested for spatial transferability and large scale applications.

As an alternative to these established image processing techniques and owing to advances in the field of machine learning, deep artificial neural networks (ANN) are becoming the model of choice for solving complex image processing tasks. Mohajerani *et al.* [28] introduced this approach by mapping calving front locations of three Greenlandic outlet glaciers using single band optical Landsat imagery emphasizing its performance, especially against hardcoded edge detection operators. Cheng *et al.* [29] substantially expanded this framework by advancing pre-processing procedures, the underlying neural network architecture as well as achieving a robust handling of Landsat-7 scanline corrector errors. Other studies focused on the usage of synthetic-aperture radar (SAR) imagery, where both single-polarization inputs [30] and dual-polarization inputs [31] have been used. While the usage of SAR has clear advantages, such as the independence from

weather and illumination, it also imposes some challenges. Particularly the backscatter characteristics of glacial ice vary throughout the year, making it hard to distinguish between relevant surfaces. Heidler *et al.* [32] addressed this problem by intertwining semantic segmentation with edge detection into a single model. They achieved better prediction performance under these problematic conditions. Considering both optical and radar sensor characteristics Zhang *et al.* [33] developed a more generalized framework capable of processing multi-sensor imagery.

Despite their similarities, all these approaches differ in study areas, input data, pre-processing strategies and neural network architecture. Recently, Heidler *et al.* [32] and Zhang *et al.* [33] provided extensive comparisons between different deep learning models and architecture modifications. However, only little consensus and literature exists regarding input feature selection and their specific contribution to prediction performance. Since remote sensing data is usually multimodal and ANN excel at synergistically integrating diverse datasets [34], we expect high potential on including additional input information. Hence, in this contribution we make an important step proposing to include further input features for automated calving front delineation from optical Landsat-8 imagery. We focus on the following three input datasets: multi-spectral bands, topographic model data and textural features. The motivation for utilizing these three datasets is given by their significance for a wide range of remote sensing tasks.

Section II covers utilized datasets and the scope of our work. Section III explains the setup and applied methods. Section IV contains the treatment of results and a subsequent discussion. Finally, Section V gives a summary and outlook.

II. DATA AND SCOPE

A. Data source

The analysis made in this paper is based on optical Landsat-8 imagery. In particular, we utilize the radiometrically calibrated and orthorectified Level-1 data products provided by the United States Geological Survey (USGS). With its two imaging sensors Operational Land Imager (OLI) and Thermal Infrared (TIR) Sensor Landsat-8 provides wide multi-spectral capabilities ranging from visible (VIS) over near-infrared (NIR) and short wave infrared (SWIR) to TIR wavelengths. In total, Landsat-8 has 11 different bands. Besides the $30\,\mathrm{m}$ resolution of the reflective bands and $100\,\mathrm{m}$ resolution of the thermal bands, an additional panchromatic band combines visible wavelengths into one channel achieving $15\,\mathrm{m}$ resolution. With the exception of band 9, which lies outside an atmospheric window and is therefore designed for observing the atmosphere, all available bands are used. In itself Landsat-8 has reasonable spatial and temporal coverage, achieving sub-weekly revisit times of all Greenlandic glaciers outside polar night. A combination with the recently launched Landsat-9 decreases revisit intervals even further, reaching sub-daily sampling for north Greenland glaciers outside polar night [35]. In the following we introduce three particular input datasets we apply in this study.

Most optical satellite-sensors capture image data within specific wavelength ranges across the electromagnetic spectrum.

Utilizing these multi-spectral bands or band combinations is widely established for glacier mapping and monitoring tasks [36]. The concept is based on the distinct reflective curves of different surface types along the electromagnetic spectrum. Figure 1 illustrates these reflectance curves for different surfaces on and around Greenland glaciers along with the atmospheric transmission and Landsat-8 band designations used in this study. Figure 2 displays these surface dependent reflectivities exemplarily for three Greenlandic glaciers: Store Glacier (a-d), Daugaard Jensen Glacier (e-h) and Jakobshavn Isbræ (i-l). The VIS spectrum (band 1-4, 8) is characterized by high reflectance of glacier ice and ice mélange as well as very high reflectance of snow [37]. Band 1 senses deep blues and violets, enabling a better view of shady surfaces than longer wavelengths. The NIR reflectivity is decreased by both grain size and the presence of liquid water [38]. The latter facilitates a better spectral separability between glacier and ice mélange. SWIR wavelengths are marked by a high reflectance of bedrock and a low reflectance of snow and ice. Signals in the TIR spectrum are influenced by thermal processes related to both surface and weather conditions [39, 40]. Depending on these conditions and the responding surface temperatures, TIR reflectivities of snow, ice and water may be very similar or noticeably different. Although some studies successfully applied multi-spectral data to facilitate automated glacier mapping [41–43], current approaches for ANN based calving front extraction are limited to the use of single band inputs, discarding additional multi-spectral information.

As a second dataset we assess topographic elevation model data. Baumhoer *et al.* [31] and Heidler *et al.* [32] already experimentally utilized a digital elevation model (DEM) and found that a careful integration facilitates more accurate model predictions. This is especially the case under challenging conditions, where synchronous topography information helps to constrain the glacier front position relative to the fjord topography. Nevertheless, Heidler *et al.* [32] also observed a severe model overfitting on the DEM for dynamic regions where elevation data and satellite imagery are contradictory. This resulted in systematic errors at the glacier front and ultimately to an accuracy decrease compared to models without DEM inputs. To counteract this, we only make use of above sea-level bed elevation. Bed elevation data has the ice thickness subtracted and is therefore temporally stationary. Thus, we avoid overfitting at the glacier front while still providing topographical context for the model. By disregarding the sub-sea-level topography, specifically by setting negative elevation values to zero, we create an ice-free DEM-like product. Bed topography data is taken from BedMachine Greenland v3 [12].

Satellite imagery of polar regions, especially in Greenland, consists mostly of natural textures. Hence our satellite images are stochastic in nature and are suitable for methods of statistical image analysis. For our third dataset, we analyze the gray-level co-occurrence matrix (GLCM), which counts the co-occurrence of neighboring gray levels in the image, enabling a statistical extraction of textural features [44]. Applying a $9\,\mathrm{px} \times 9\,\mathrm{px}$ sliding window on the $15\,\mathrm{m}$ resolution panchromatic band we extract the following textural features: angular second moment, contrast, entropy, dissimilarity, homogeneity
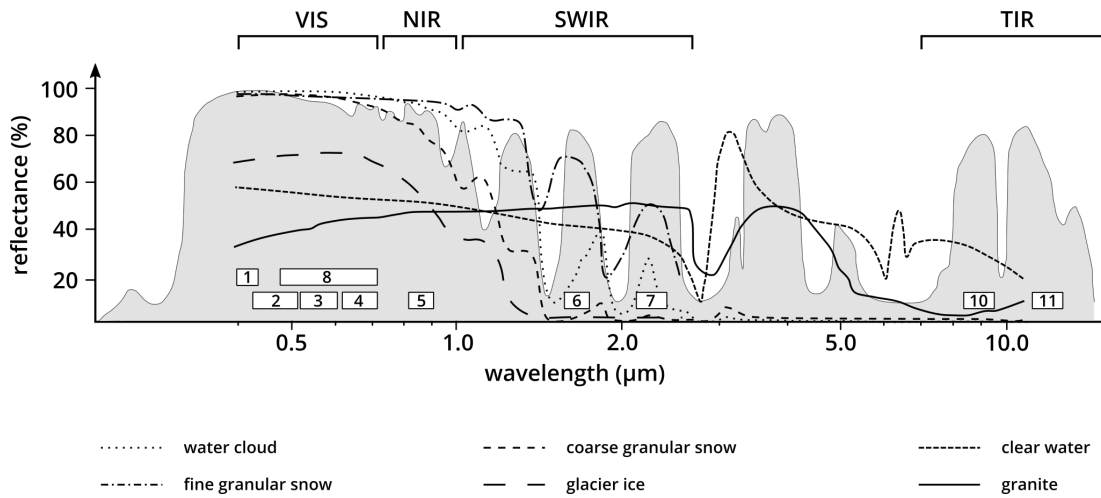
Fig. 1. Atmospheric transmission, Landsat-8 band designations (numbers) and typical reflectance curves for different surfaces found on or around glaciers. Figure adapted from Kääb *et al.* [36].
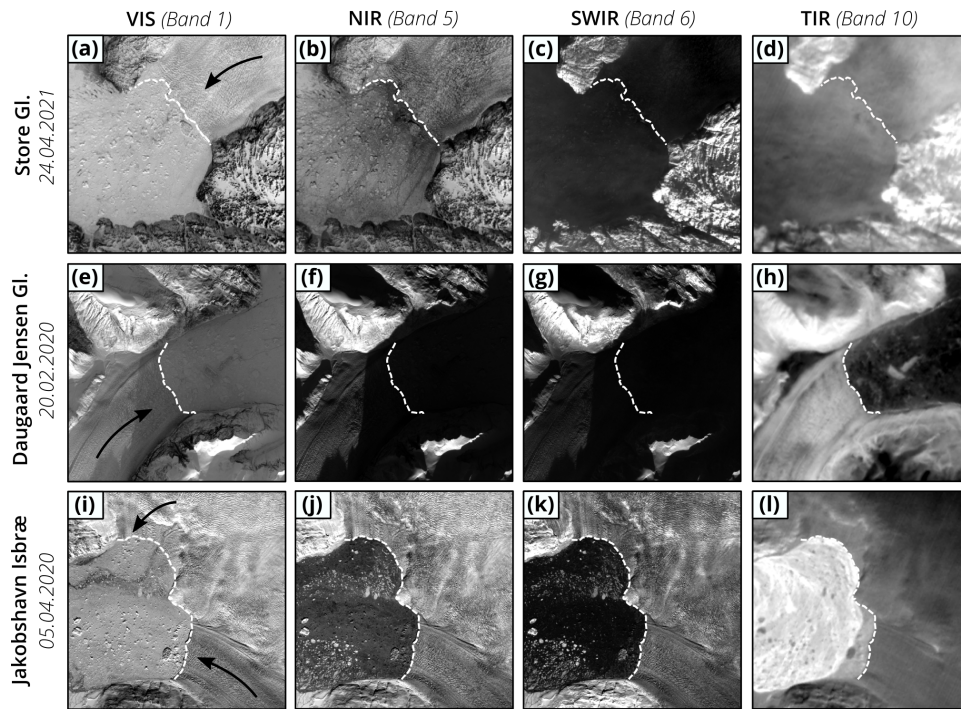

Fig. 2. Surface dependent reflectivities for Store Glacier (a-d), Daugaard Jensen Glacier (e-h) and Jakobshavn Isbræ (i-l) for different wavelength ranges of Landsat-8, namely the deep blue (Band 1), NIR (Band 5), SWIR (Band 6) and TIR (Band 10). Arrows indicate ice flow direction. The calving front is highlighted as a dashed line. For the location of the specific glaciers see Fig. 4.

and correlation. The idea in utilizing these features is that the homogeneous texture of the ice mélange, water or fast ice stands out to the glacier front which is characterized by crevasses, seracs and other distinguishing features [25]. Figure 3 emphasizes this aspect by showing (a) the panchromatic image, (b-g) spatial characteristics of GLCM textural features and (h) the topography model exemplarily for Hagen Bræ in North Greenland (Fig. 4). Although the textural features allow for a better separability between different surface types, they do not well represent objects or areas smaller than the selected window size. In Figure 3 this is particularly evident for the small icebergs near the glacier front. Reducing the window size further would enable a sharper transition between relevant surface types, but also leads to a noisy and unstable feature extraction. Since the GLCM feature transformation is highly non-linear, it cannot be learned easily by neural networks and can thus provide a valuable enrichment of the input data. Combining GLCM textural features with ANNs has therefore already been explored in various areas of image analysis [45–47]. Here we will assess how this method can be applied for the calving front extraction.
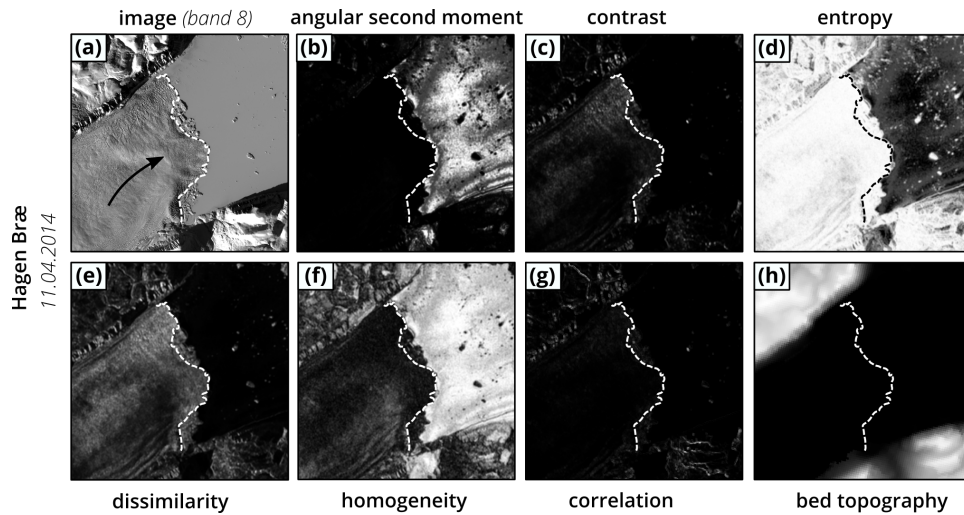
Fig. 3. (a) Panchromatic image, (b-g) textural features and (h) above-sea level topography of Hagen Bræ. Arrows indicate ice flow direction. The calving front is highlighted as a dashed line.

B. Reference dataset

Over the last two decades the Greenland Ice Sheet has experienced an increased ice-mass loss which is caused mainly due to increased surface melt and ice discharge [48]. Along with accelerating glacier velocity and frontal ablation, high retreat rates have been found [2]. The quantification and understanding of glacier dynamics will provide important insights into the Greenland Ice Sheet response to ongoing change as well as long-term climate forcing. In order to facilitate these analyses and resolve spatial and temporal data gaps of calving front positions, we choose the Greenland Ice Sheet as the main study area for our assessment.

Our reference dataset consists of 18 Greenland outlet glaciers which are used for model training, validating and testing. Additional 5 Greenlandic glaciers and 2 glaciers at the Antarctic Peninsula are used for model testing, specifically for assessing spatial transferability. Figure 4 gives an overview of the spatial distribution of our analyzed glaciers. The selection ensures diversity of morphological features as well as of calving and ocean conditions. As these conditions also change throughout the year with cloud cover and illumination changing scene by scene, we have to ensure sufficient sampling during the observation periods from spring to autumn. In total, the reference dataset consists of 728 manually delineated calving front positions, of which 585 calving fronts (from 2013 to 2019) are used as input for model training, and 143 calving fronts (from 2020 and 2021) are used for model testing.

III. METHODS

A. Neural network implementation

Mapping glacier calving front locations is a contour detection task. So far the most popular approach in accomplishing this with ANNs is based on pixel-wise semantic image segmentation using a convolutional neural network followed by vectorizing the output mask. In particular U-Net type architectures [49] have proven to be very effective for various study areas and sensor types [28, 30–32]. Since this study focuses on input data assessment rather than advancing ANN architecture, we adapt the already established U-Net model for our analysis. The U-Net itself is based on a contracting path reducing spatial information while increasing feature information followed by an expanding path where spatial and feature information are combined by alternating concatenations and deconvolutions. The receptive field of a U-Net is defined by the number of contracting and expanding blocks. Deeper models have larger receptive fields and thereby more spatial context information for each pixel classification. Since calving front delineation benefits significantly from increased spatial context [32] our model is expanded by two additional resolution levels, i.e. from four to six levels. Figure 5 shows the processing architecture and relevant dimensions of the U-Net used in this study.

The presented model performs a land surface classification where a land and glacier class is semantically segmented from a water class, with the calving front later to be extracted from the boundary between these two classes. The ANN input consists of the multi-spectral, topographic and textural datasets described in Section II. Raster subsets have dimensions of $512\,\text{px} \times 512\,\text{px}$ and are centered at the calving front location of the corresponding glacier. With a uniformly applied $30\,\text{m}$ ground sampling distance each input raster subset covers an area of about $15\,\text{km} \times 15\,\text{km}$. To counteract overexposed areas in our satellite imagery we apply additional image enhancement in form of a cumulative count cut clipping the data between the 0.1 and 98 percentile of each multi-spectral band. In total, we use 17 input layers, namely 10 Landsat-8 bands, 6 GLCM textural features and bed topography. Finally, all of these 17 input layers are normalized to the range between 0 and 1 using an 8-Bit quantization.

To counteract model overfitting we select every fifth image of the training data, a total of 164, for internal validation. The remaining training data is augmented 8-fold by flipping and rotating. The resulting 5232 raster subsets are finally used for training the model with randomized batches of size 8. For this we apply the Adam optimization algorithm [50] on a
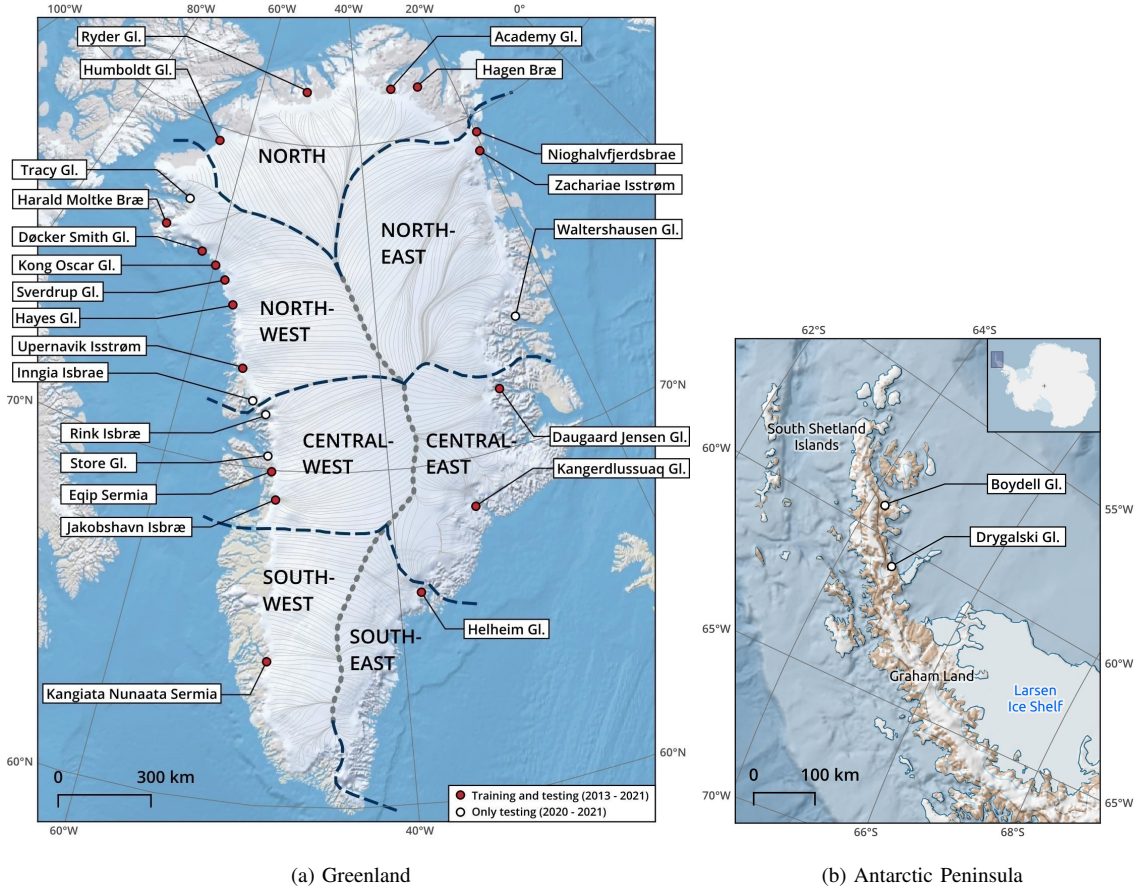
(a) Greenland   (b) Antarctic Peninsula

Fig. 4. Geographic location of the 23 Greenlandic and the 2 Antarctic outlet glaciers used in our reference dataset. Red dots indicate glaciers used for training and testing. Glaciers marked with a white dot are only used for model testing.

binary cross-entropy loss function for 150 epochs. The final model weights are selected based on the binary classification accuracy of the internal validation dataset. The ANN implementation is realized using the TensorFlow 2.3 library [51]. Training is carried out on an IBM Power 9 node using a NVIDIA V100 GPU with 32 GB high bandwidth memory. With each epoch taking three to four minutes, our model is trained after 7.5 to 10 hours. Up to 32 models can be trained in parallel.

Figure 6 gives a basic overview of the processing workflow. The trained model performs an automated land surface classification, where each image pixel is denoted a probability between 0 (water) and 1 (glacier and land). As part of post-processing, this floating point number probability mask is vectorized using the Geospatial Data Abstraction Library contour algorithm [52], thresholding at a probability of 0.5. Larger glaciers, with calving fronts exceeding the $512\,\text{px} \times 512\,\text{px}$ input window, are separated into several independent predictions which are averaged in the overlapping area before vectorization. This concept is adopted from Baumhoer *et al.* [31]. It is applied for Humboldt Glacier, Nioghalvfjerdsbræ and Zachariae Isstrøm, which are split into 7, 3, and 2 separate overlapping predictions, respectively. Finally, we extract the glacier calving front by intersecting the vectorized coastline with a static mask. This mask is manually created for each

glacier and specifies the corridor of possible calving front locations.

B. Accuracy assessment

To validate the ANN model it was applied to the test dataset introduced in Section II-B. This test dataset contains 177 manually delineated frontal positions for all Greenlandic glaciers used for training the model, but for the different time period 2020 and 2021. Also included were an additional 5 Greenlandic glaciers and 2 glaciers at the Antarctic Peninsula.

As main error metric we choose the distance between the predicted and the manually delineated calving front trajectory. Conceptually, this corresponds to the area between the two curves normalized by their length. We implement this metric by averaging the minimal distance to the manual delineation every 30 m along the predicted front. We define two different accuracy estimates based on the non-normal distribution of the averaged distance error for the 177 test scenes:

1) The *mean distance error* is sensitive towards outliers, which are mostly due to large misclassified areas and therefore falsely extracted calving front positions of scenes with very challenging conditions.

2) The *median distance error*, in contrast, is not sensitive towards individual scenes. It gives information on the
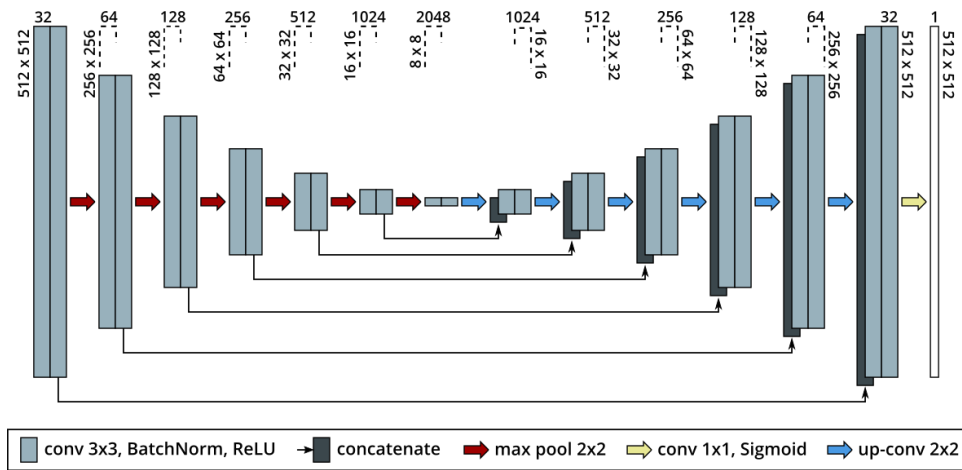
Fig. 5. The U-Net based processing architecture used in this study. A contracting sequence consists of convolutions followed by batch normalization, a rectified linear unit (ReLU) and a max pooling operation. Expanding sequences are composed of a concatenation with spatial context from the contracting path, convolutions followed by batch normalization and a ReLU. Note that all dimensions are denoted at the top of the blocks.
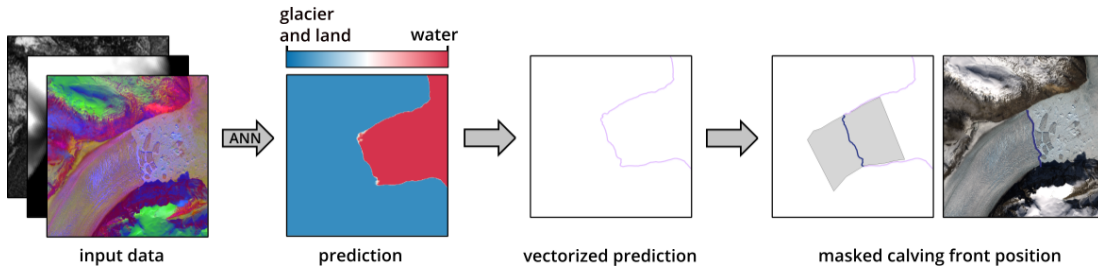

Fig. 6. Overview of the processing workflow using an exemplary satellite scene of the Daugaard Jensen Glacier. Through an ANN, a land and glacier class is semantically segmented from a water class. After vectorization, we extract the calving front using a static mask.

general scene-by-scene performance as well as on a systematic overfitting of our model.

Although our model is fitted using pixel-wise binary cross-entropy, the mean and median distance error metrics are more representative measures of model performance. This is due to the ANN based pixel-wise classification only being an intermediate step in our processing scheme. A high binary classification accuracy does not necessarily translate into an accurate calving front prediction as binary classification accuracy is primarily important directly at the glacier front.

C. Assessment of feature importance

Deep learning has proven to be a powerful set of tools in many data-driven fields. However, these methods often produce complex models that provide little to no insight how these predictions are derived. Numerous methods are attempting to look inside this "black box" function and to understand the contribution of a feature to the predictive power of a model. Popular and computational convenient methods are based on the *permute-and-predict* strategy first introduced by Breiman [53]. Since our model inputs exhibit significant statistical dependences, which is a common property of multi-layer remote sensing imagery, diagnostics based on this *permute-and-predict* approach can be highly misleading [54–56]. Hooker and Mentch [57] explain this behavior in detail and suggest several alternatives generally based on

either conditional permutation or model-relearning. Taking the results of these studies into account, we evaluate our features using the *dropped variable* concept suggested by Hooker and Mentch [57], which is equivalent to the *leave one covariate out* framework introduced by Lei *et al.* [58].

For this we re-train the ANN model applying only certain subsets of our input features. The prediction power of these models, in this study portrayed by the mean and median distance error to the manual delineation, is then comparatively evaluated. This very pragmatic approach allows us to conclude on the benefit of corresponding omitted or supplemented input features. Rather than evaluating every layer separately we use the three input datasets introduced in Section II: multi-spectral bands, topographic model data and textural features. This is computationally feasible and coherent from a user implementation point of view. Since we want to assess the contribution of each dataset compared to conventional single band input, the panchromatic band is always included.

ANN training is not deterministic; instead, it is stochastic. Even when using the same training data, every fitted model is different and therefore performs differently when applied to the test dataset. This is especially prevalent in our workflow since the loss function used to optimize the model differs from the error metric used in accuracy assessment. A better model convergence could be achieved by applying a custom loss function as well as by implementing additional output
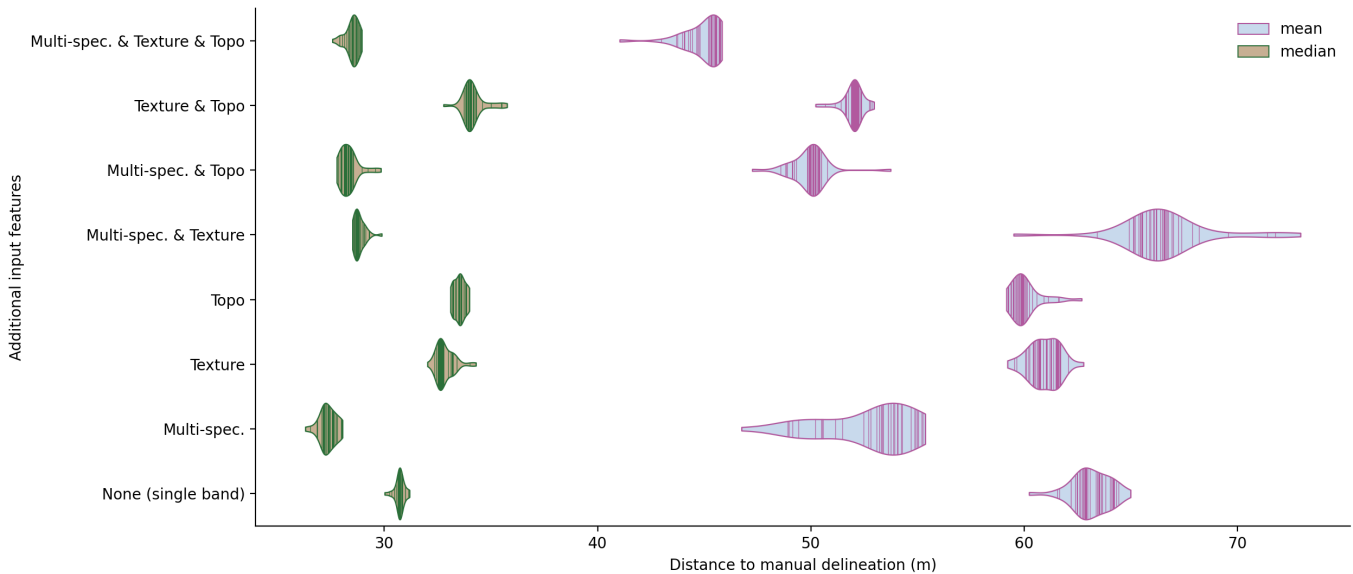
Fig. 7. Results of the feature importance assessment. The various input feature combinations are listed on the Y-axis, with the panchromatic single band image being supplemented by additional features. The 'violin plot' depicts the distribution of mean distance error and median distance error assessed by comparison to the manual calving front delineation. Every vertical line represents one trained model applied on the test dataset. The horizontal extent of the 'violin graphs' is defined by corresponding minimum and maximum values and the vertical extent by the frequency distribution.

TABLE I
MEAN AND MEDIAN DISTANCE ERROR AS WELL AS BINARY CLASSIFICATION METRICS ACCURACY AND F1-SCORE FOR DIFFERENT COMBINATIONS OF INPUT DATA.

Additional input features	Mean distance (m)	Median distance (m)	Binary classification accuracy	F1-Score
Multi-spec. & Texture & Topo	(44.9 ± 0.9)	(28.6 ± 0.5)	(99.10 ± 0.04)	(99.31 ± 0.03)
Texture & Topo	(52.0 ± 0.5)	(34.2 ± 0.5)	(99.08 ± 0.01)	(99.30 ± 0.01)
Multi-spec. & Topo	(49.9 ± 0.9)	(28.3 ± 0.4)	(99.05 ± 0.04)	(99.27 ± 0.03)
Multi-spec. & Texture	(66.5 ± 2.0)	(28.8 ± 0.3)	(98.32 ± 0.07)	(98.74 ± 0.04)
Topo	(60.0 ± 0.7)	(33.5 ± 0.3)	(99.01 ± 0.04)	(99.25 ± 0.02)
Texture	(60.9 ± 0.7)	(32.8 ± 0.4)	(98.47 ± 0.07)	(98.83 ± 0.04)
Multi-spec.	(52.7 ± 2.2)	(27.4 ± 0.4)	(98.68 ± 0.04)	(99.00 ± 0.03)
None (single band)	(63.1 ± 0.9)	(30.7 ± 0.2)	(98.45 ± 0.07)	(98.82 ± 0.06)

layers, which enforce calving front classification more heavily. In this analysis, we enable a thorough comparison between the different input datasets by fitting 40 models for each feature combination. This ensures statistical stability and an estimate for the variability of the predictions.

IV. RESULTS AND DISCUSSION

Figure 7 presents the outcome of the feature importance analysis. Mean and median distance errors are depicted for various input feature combinations. Each vertical line inside the 'violin graphs' represents one trained model applied to the test dataset. Table I lists corresponding statistics. It also quotes the binary classification metrics accuracy and F1-score for comparability to existing studies [31, 32]. Regardless of the applied feature set, the median error is always smaller than the mean error. This is due to some challenging test scenes which exhibit large deviations to the manual delineation. The mean error characterizes the predictive power of a model under these conditions. When using the panchromatic band only, without additional input features, the trained models provide reliable predictions with $63\,\text{m}$ mean and $31\,\text{m}$ median error for our test dataset (last line in Fig. 7 and Table I). Additional input

features can both increase and decrease a model's predictive power. For the median error, an improvement in model performance with respect to conventional single band processing is only observed when applying multi-spectral features. In contrast, the median error increases if textural and/or topography data are added without adding multi-spectral features. This indicates that both of these datasets can increase a models susceptibility for overfitting which lead to systematic misclassifications at the calving front throughout the whole test dataset. Notably, models using only multi-spectral features have a slightly better median performance compared to models using all available data. Evaluating the mean distance error of our models enables an assessment on the handling of challenging scenes as the mean is particularly sensitive towards outliers. With the exception of combining multi-spectral with textural inputs, all assessed models exhibit an improvement in mean error with respect to the single band processing. Combining all three presented datasets results in a significant mean error decrease from $63\,\text{m}$ to $45\,\text{m}$, emphasizing their benefit for processing imagery under challenging conditions.

Figure 8 presents specific examples of the above concluded characteristics. Each of the 40 model predictions is shown in
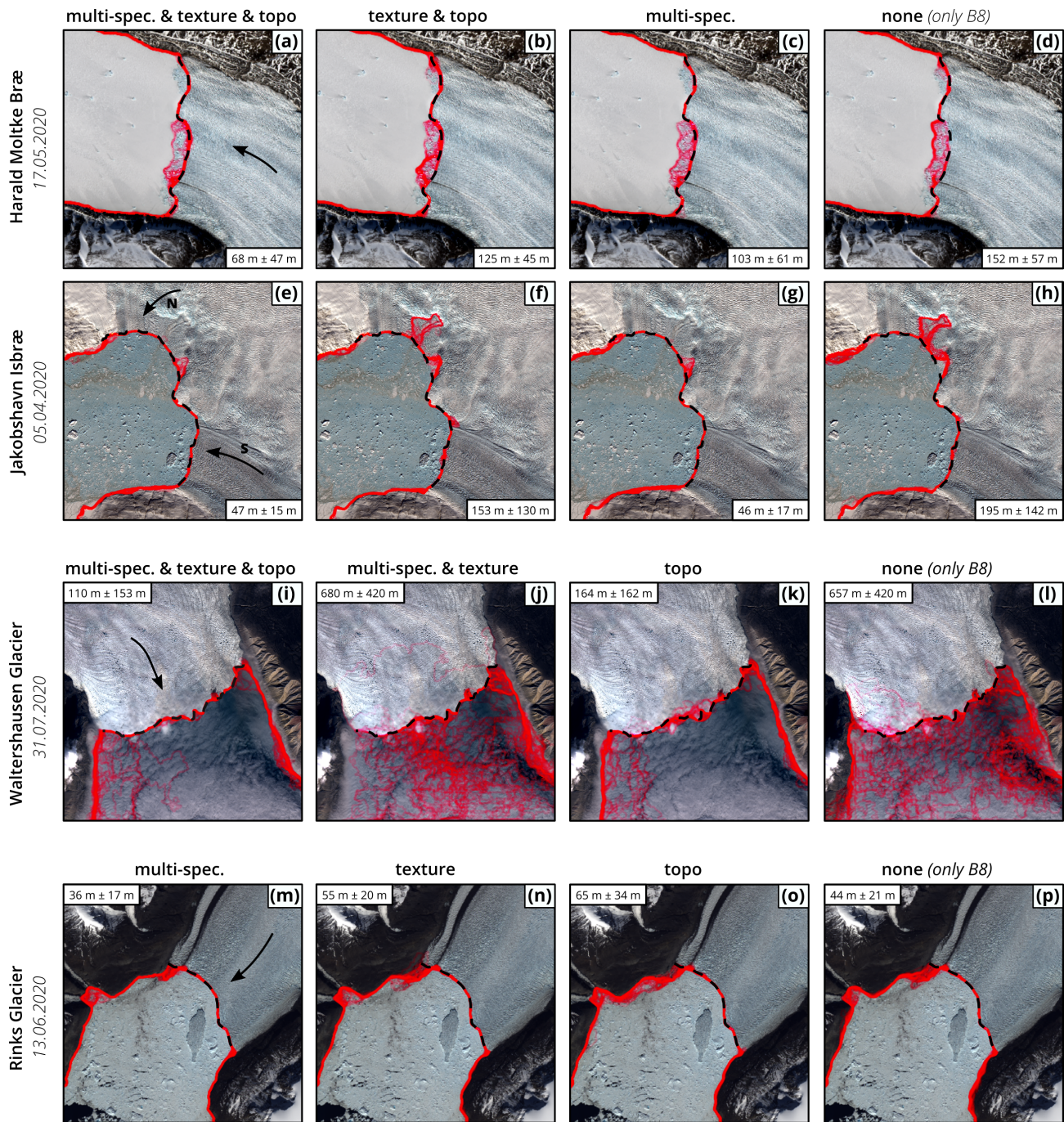
Fig. 8. Feature importance exemplarily shown for four different test scenes. Shown are RGB images with ground truth as dashed black line, ice flow direction as an arrow and the 40 model predictions in semi-transparent red for different glaciers (rows) and different input features denoted above the respective columns. The mean distance error for the depicted predictions at the glacier front is also given.

semi-transparent red with increasing intensity the more the predictions overlap. The manually delineated front position is drawn as a dashed black line. The presence of fast ice usually leads to abrupt textural changes ahead of the actual glacier front. This is a result of the fast ice breaking at the glacier front or calved ice which is not transported away. Conditions like these often lead to systematic misclassifications of the ANN since both gray value and texture help very little in differentiating these surfaces. This causes the predicted front to follow the wrong textural transition and

results in a large distance error. The case of Harald Moltke Bræ (Fig. 8a-d) demonstrates these characteristics and confirms a significant accuracy increase by including multi-spectral information. This is a result of varying reflectivities of different ice, snow and ice-melange surfaces. Figure 8 (e-h), showing a scene of Jakobshavn Isbræ, manifests the same aspect in a slightly different way. Frequent breakups of the northern branch terminus lead to an unpronounced textural transition at the calving front. Without utilizing multi-spectral information, these scenes remain very hard to delineate. The third scene

(Fig. 8i-l), shows the performance using different input feature sets at Waltershausen Glacier. Thick clouds cover most of the scene and barely allow us to identify the calving front. Combined with the fact that this glacier is not part of the training dataset, this scene is very challenging to process by the ANN. The different models clearly show that under conditions like these, stable predictions are only possible using topography data. In particular, the calving front - coastline transition as well as large parts of the coastline itself are not visible in this scene, thus making external data mandatory for an accurate delineation. Topographic information provides an important constraint of the calving front position inside the fjord. Finally, the case of Rinks Glacier (Fig. 8m-p) is representative of a large portion of the test imagery which is reliably delineated, with distance errors well below $100\,\mathrm{m}$, regardless of the used input information. Still, we notice a decreased distance error when applying multi-spectral data. Interestingly, but also in accordance with our findings in Figure 7, the addition of textural as well as topography data increases the distance error. This happens for a large number of otherwise easy to delineate test scenes, and mostly for certain parts of the glacier front with changing ice-melange texture or pronounced glacial meltwater plumes. Hence, we suspect increased overfitting when including textural and topography data which manifests in a larger median error over the whole dataset. Although we applied several techniques to counteract model overfitting, modifying the ANN architecture, specifically adjusting its complexity, might be necessary to take full advantage of these input features.

V. SUMMARY AND OUTLOOK

Our results provide important insights for advancing ANN based calving front extraction. The feature importances portrayed in this study emphasize both the potential in integrating additional input information as well as the significance of their thoughtful selection. The integration of multi-spectral bands is not only convenient since most data products deliver this information anyway, but also leads to more accurate predictions especially under challenging conditions. Using topography and textural inputs cannot be recommended without reservation. Both datasets can help for certain scenes but result in a higher median distance error for our test dataset, which indicates that the corresponding models are overfitted. The integration of these datasets needs to be done carefully and, if possible, accompanied by further investigations and model adjustments.

The results of this assessment are not only relevant for advancing automated calving front extraction, but also for a wider range of glaciological land surface classification tasks using optical imagery and deep neural networks. Recent studies already explored the application of deep learning algorithms for mapping supraglacial lakes and debris-covered glaciers. The results presented in our contribution reinforce these existing efforts but also lay the foundation for further applications and developments.

CODE AND DATA AVAILABILITY

The code used for pre-processing, ANN training and accuracy assessment as well as all reference data applied in this study are available at the TU Dresden Open Access Repository and Archive (http://dx.doi.org/10.25532/OPARA-183). In particular, this includes 728 manually delineated calving front positions, which we provide in a georeferenced shapefile format, as well as 995 machine learning ready input raster subsets with their corresponding, manual delineated, segmentation mask.

REFERENCES

[1] I. Joughin, I. Howat, R. B. Alley, G. Ekstrom, M. Fahnestock, T. Moon, M. Nettles, M. Truffer, and V. C. Tsai, "Ice-front variation and tidewater behavior on Helheim and Kangerdlugssuaq Glaciers, Greenland," *Journal of Geophysical Research: Earth Surface*, vol. 113, no. F1, 2008.

[2] T. Moon and I. Joughin, "Changes in ice front position on Greenland's outlet glaciers from 1992 to 2007," *Journal of Geophysical Research: Earth Surface*, vol. 113, no. F2, 2008.

[3] L. Müller, M. Horwath, M. Scheinert, C. Mayer, B. Ebermann, D. Floricioiu, L. Krieger, R. Rosenau, and S. Vijay, "Surges of Harald Moltke Bræ, north-western Greenland: seasonal modulation and initiation at the terminus," *The Cryosphere*, vol. 15, no. 7, pp. 3355 – 3375, 2021.

[4] D. I. Benn, T. Cowton, J. Todd, and A. Luckman, "Glacier Calving in Greenland," *Current Climate Change Reports*, vol. 3, pp. 282 – 290, 2017.

[5] D. A. Slater, F. Straneo, D. Felikson, C. M. Little, H. Goelzer, X. Fettweis, and J. Holte, "Estimating greenland tidewater glacier retreat driven by submarine melting," *The Cryosphere*, vol. 13, no. 9, pp. 2489–2509, 2019. [Online]. Available: https://tc.copernicus.org/articles/13/2489/2019/

[6] M. Trevers, A. J. Payne, S. L. Cornford, and T. Moon, "Buoyant forces promote tidewater glacier iceberg calving through large basal stress concentrations," *The Cryosphere*, vol. 13, no. 7, pp. 1877–1887, 2019. [Online]. Available: https://tc.copernicus.org/articles/13/1877/2019/

[7] S. J. Cook, P. Christoffersen, M. Truffer, T. R. Chudley, and A. Abellán, "Calving of a large greenlandic tidewater glacier has complex links to meltwater plumes and mélange," *Journal of Geophysical Research: Earth Surface*, vol. 126, no. 4, p. e2020JF006051, 2021, e2020JF006051 2020JF006051. [Online]. Available: https://agupubs.onlinelibrary.wiley.com/doi/abs/10.1029/2020JF006051

[8] S. M. Melton, R. B. Alley, S. Anandakrishnan, B. R. Parizek, M. G. Shahin, L. A. Stearns, A. L. LeWinter, and D. C. Finnegan, "Meltwater drainage and iceberg calving observed in high-spatiotemporal resolution at helheim glacier, greenland," *Journal of Glaciology*, p. 1–17, 2022.

[9] R. B. Alley, J. Andrews, J. Brigham-Grette, G. Clarke, K. Cuffey, J. Fitzpatrick, S. Funder, S. Marshall, G. Miller, J. Mitrovica, D. Muhs, B. Otto-Bliesner, L. Polyak, and J. White, "History of the greenland ice sheet: paleoclimatic insights," *Quaternary Science Reviews*, vol. 29, no. 15, pp. 1728 –1756, 2010, special Theme: Arctic Palaeoclimate Synthesis (PP. 1674-1790). [Online]. Available: https://www.sciencedirect.com/science/article/pii/S0277379110000399

[10] A. Vieli and F. M. Nick, "Understanding and modelling rapid dynamic changes of tidewater outlet glaciers: Issues and implications," *Surveys in Geophysics volume*, vol. 32, pp. 437 – 458, 2011.

[11] J. H. Bondizo, M. Morlighem, H. Seroussi, T. Kleiner, M. Rückamp, J. Mouginot, T. Moon, E. Y. Larour, and A. Humbert, "The mechanisms behind Jakobshavn Isbræ's acceleration and mass loss: A 3-D thermomechanical model study," *Geophysical Research Letters*, vol. 44, no. 12, pp. 6252–6260, 2017.

[12] M. Morlighem, C. N. Williams, E. Rignot, L. An, J. E. Arndt, J. L. Bamber, G. Catania, N. Chauché, J. A. Dowdeswell, B. Dorschel, I. Fenty, K. Hogan, I. Howat, A. Hubbard, M. Jakobsson, T. M. Jordan, K. K. Kjeldsen, R. Millan, L. Mayer, J. Mouginot, B. P. Y. Noël, C. O'Cofaigh, S. Palmer, S. Rysgaard, H. Seroussi, M. J. Siegert, P. Slabon, F. Straneo, M. R. van den Broeke, W. Weinrebe, M. Wood, and K. B. Zinglersen, "BedMachine v3: Complete Bed Topography and Ocean Bathymetry Mapping of Greenland From Multibeam Echo Sounding Combined With Mass Conservation," *Geophysical Research Letters*, vol. 44, no. 21, pp. 11 051 – 11 061, 2017.

[13] M. Morlighem, M. Wood, H. Seroussi, Y. Choi, and E. Rignot, "Modeling the response of northwest greenland to enhanced ocean thermal forcing and subglacial discharge," *The Cryosphere*, vol. 13, no. 2, pp. 723–734, 2019. [Online]. Available: https://tc.copernicus.org/articles/13/723/2019/

[14] H. Goelzer, S. Nowicki, A. Payne, E. Larour, H. Seroussi, W. H. Lipscomb, J. Gregory, A. Abe-Ouchi, A. Shepherd, E. Simon, C. Agosta, P. Alexander, A. Aschwanden, A. Barthel, R. Calov, C. Chambers, Y. Choi, J. Cuzzone, C. Dumas, T. Edwards, D. Felikson, X. Fettweis, N. R. Golledge, R. Greve, A. Humbert, P. Huybrechts, S. Le clec'h, V. Lee, G. Leguy, C. Little, D. P. Lowry, M. Morlighem, I. Nias, A. Quiquet, M. Rückamp, N.-J. Schlegel, D. A. Slater, R. S. Smith, F. Straneo, L. Tarasov, R. van de Wal, and M. van den Broeke, "The future sea-level contribution of the greenland ice sheet: a multi-model ensemble study of ismip6," *The Cryosphere*, vol. 14, no. 9, pp. 3071–3096, 2020. [Online]. Available: https://tc.copernicus.org/articles/14/3071/2020/

[15] R. Williams, J. Ferrigno, C. Swithinbank, B. Lucchitta, and B. Seekins, "Coastal-change and glaciological maps of Antarctica," *Annals of Glaciology*, vol. 21, pp. 284 – 290, 1995.

[16] I. Joughin, T. Moon, and T. Black, "MEaSUREs Annual Greenland Outlet Glacier Terminus Positions from SAR Mosaics, Version 1," *Boulder, Colorado USA. NASA National Snow and Ice Data Center Distributed Active Archive Center*, 2015, (last access: 11.November 2021).

[17] ENVEO, "Greenland Calving Front Dataset, 1990–2016, v3.0," 2017, (last access: 11.November 2021). [Online]. Available: http://products.esa-icesheets-cci.org/products/downloadlist/CFL

[18] J. A. Andersen, R. S. Fausto, K. Hansen, J. E. Box, S. B. Andersen, A. P. Ahlstrøm, D. van As, M. Citterio, W. Colgan, N. B. Karlsson, K. K. Kjeldsen, N. J. Korsgaard, S. H. Larsen, K. D. Mankoff, A. Ø. Pedersen, C. L. Shields, A. Solgaard, and B. Vandecrux, "Update of annual calving front lines for 47 marine terminating outlet glaciers in Greenland (1999–2018)," *GEUS Bulletin*, vol. 43, 2019, (last access: 11.November 2021).

[19] G. Moholdt, J. Maton, M. Majerska, and J. Kohler, "Annual frontlines of marine-terminating glaciers on Svalbard [Data set]," *Norwegian Polar Institute*, 2021, (last access: 11.November 2021).

[20] SCAR Antarctic Digital Database, "BAS Data Catalogue, SCAR Antarctic Digital Database (ADD)," 2021, (last access: 11.November 2021). [Online]. Available: https://data.bas.ac.uk/collections/e74543c0-4c4e-4b41-aa33-5bb2f67df389

[21] CPOM, "Centre of Polar Observation and Modelling Data Portal, Monitoring ice shelves in Antarctica," 2021, (last access: 11.November 2021). [Online]. Available: http://www.cpom.ucl.ac.uk/csopr/brunt

[22] H. G. Sohn and K. C. Jezek, "Mapping ice sheet margins from ERS-1 SAR and SPOT imagery," *International Journal of Remote Sensing*, vol. 20, no. 15-16, pp. 3201 – 3216, 1999.

[23] H. Liu and K. C. Jezek, "A Complete High-Resolution Coastline of Antarctica Extracted from Orthorectified Radarsat SAR Imagery," *Photogrammetric Engineering and Remote Sensing*, vol. 5, no. 12, pp. 605 – 616, 2004.

[24] A. Seale, P. Christoffersen, R. I. Mugford, and M. O'Leary, "Ocean forcing of the Greenland Ice Sheet: Calving fronts and patterns of retreat identified by automatic satellite monitoring of eastern outlet glaciers," *Journal of Geophysical Research: Earth Surface*, vol. 116, no. F3, 2011.

[25] R. Rosenau, "Untersuchung von fließgeschwindigkeit und frontlage der großen ausflussgletscher grönlands mittels multitemporaler landsat-aufnahmen," Ph.D. dissertation, Technische Universität Dresden, Qucosa, 2014, urn:nbn:de:bsz:14-qucosa-138514.

[26] L. Krieger and D. Floricioiu, "Automatic calving front delienation on TerraSAR-X and Sentinel-1 SAR imagery," *International Geoscience and Remote Sensing Symposium (IGARSS)*, 2017.

[27] J. Liu, E. M. Enderlin, H.-P. Marschall, and A. Khalil, "Automated Detection of Marine Glacier Calving Fronts

Using the 2-D Wavelet Transform Modulus Maxima Segmentation Method," *IEEE Transactions on Geoscience and Remote Sensing*, vol. 59, no. 11, pp. 9047 – 9056, 2021.

[28] Y. Mohajerani, M. Wood, I. Velicogna, and E. Rignot, "Detection of Glacier Calving Margins with Convolutional Neural Networks: A Case Study ," *Remote Sensing*, vol. 11, no. 1, p. 74, 2019.

[29] D. Cheng, W. Hayes, E. Larour, Y. Mohajerani, M. Wood, I. Velicogna, and E. Rignot, "Calving Front Machine (CALFIN): Glacial Termini Dataset and Automated Deep Learning Extraction Method for Greenland, 1972–2019 ," *The Cryosphere*, vol. 15, no. 3, 2021.

[30] E. Zhang, L. Liu, and L. Huang, "Automatically delineating the calving front of Jakobshavn Isbræ from multitemporal TerraSAR-X images: a deep learning approach," *The Cryosphere*, vol. 13, no. 6, p. 1729–1741, 2019.

[31] C. A. Baumhoer, A. J. Dietz, C. Kneisel, and C. Kuenzer, "Automated Extraction of Antarctic Glacier and Ice Shelf Fronts from Sentinel-1 Imagery Using Deep Learning," *Remote Sensing*, vol. 11, no. 21, p. 2529, 2019.

[32] K. Heidler, L. Mou, C. Baumhoer, A. Dietz, and X. X. Zhu, "Hed-unet: Combined segmentation and edge detection for monitoring the antarctic coastline," *IEEE Transactions on Geoscience and Remote Sensing*, 2021.

[33] E. Zhang, L. Liu, L. Huang, and K. S. Ng, "An automated, generalized, deep-learning-based method for delineating the calving fronts of Greenland glaciers from multi-sensor remote sensing imagery," *Remote Sensing of Environment*, vol. 254, p. 112265, 2021.

[34] X. X. Zhu, D. Tuia, L. Mou, G.-S. Xia, L. Zhang, F. Xu, and F. Frauendorfer, "Deep Learning in Remote Sensing: A Comprehensive Review and List of Resources," *IEEE Geoscience and Remote Sensing Magazine*, vol. 5, no. 4, pp. 8–36, 2017.

[35] J. Li and B. Chen, "Global Revisit Interval Analysis of Landsat-8 -9 and Sentinel-2A -2B Data for Terrestrial Monitoring," *Sensors*, vol. 20, no. 22, p. 6631, 2020.

[36] A. Kääb, T. Bolch, K. Casey, T. Heid, J. S. Kargel, G. J. Leonard, F. Paul, and B. H. Raup, "Glacier mapping and monitoring using multispectral data," in *Global Land Ice Measurements from Space*, J. S. Kargel, G. J. Leonard, M. P. Bishop, A. Kääb, and B. H. Raup, Eds. Heidelberg: Springer, 2014, ch. 4, pp. 75–112.

[37] S. G. Warren and R. E. Brandt, "Optical constants of ice from the ultraviolet to the microwave: A revised compilation," *Journal of Geophsical Research: Atmospheres*, vol. 113, no. D14, 2008.

[38] H. Rott, "Analyse der Schneeflächen auf Gletschern der tiroler Zentralalpen aus Landsat-Bildern," *Zeitschrift für Gletscherkunde und Glazialgeologie*, vol. 12, no. 1, pp. 1 – 28, 1976.

[39] Y. Wu, N. Wang, J. He, and X. Jiang, "Estimating mountain glacier surface temperatures from Landsat-ETM + thermal infrared data: A case study of Qiyi glacier, China," *Remote Sensing of Environment*, vol. 163, pp. 286 – 295, 2015.

[40] H. Liao, Q. Liu, Y. Zhong, and X. Lu, "Landsat-Based Estimation of the Glacier Surface Temperature of Hailuogou Glacier, Southeastern Tibetan Plateau, Between 1990 and 2018," *Remote Sensing of Environment*, vol. 12, no. 13, p. 2105, 2020.

[41] A. E. Racoviteanu, M. W. Willialms, and R. G. Barry, "Optical Remote Sensing of Glacier Characteristics: A Review with Focus on the Himalaya," *Sensors*, vol. 8, no. 5, pp. 3355 – 3383, 2008.

[42] E. Gjermundsen, R. Mathieu, A. Kääb, T. Chinn, B. Fitzharris, and J. Hagen, "Assessment of multispectral glacier mapping methods and derivation of glacier area changes, 1978–2002, in the central Southern Alps, New Zealand, from ASTER satellite data, field survey and existing inventory data," *Journal of Glaciology*, vol. 57, no. 204, pp. 667 – 683, 2011.

[43] D. J. Selkowitz and R. R. Forster, "Automated mapping of persistent ice and snow cover across the western U.S. with Landsat," *ISPRS Journal of Photogrammetry and Remote Sensing*, vol. 117, pp. 126 – 140, 2016.

[44] R. M. Haralick, K. Shanmugam, and I. Dinstein, "Textural Features for Image Classification," *IEEE Transactions on Systems, Man, and Cybernetics*, vol. SMC-3, no. 6, pp. 610 – 621, 1973.

[45] J. Rahebi and F. Hardalaç, "Retinal Blood Vessel Segmentation with Neural Network by Using Gray-Level Co-Occurrence Matrix-Based Features," *Journal of Medical Systems*, vol. 35, p. 85, 2014.

[46] M. Pratiwi, Alexander, J. Harefa, and S. Nanda, "Mammograms Classification Using Gray-level Co-occurrence Matrix and Radial Basis Function Neural Network," *Procedia Computer Science*, vol. 59, pp. 83 – 91, 2015.

[47] M. M. Santoni, D. I. Sensuse, A. M. Arymurthy, and M. I. Fanany, "Cattle Race Classification Using Gray Level Co-occurrence Matrix Convolutional Neural Networks," *Procedia Computer Science*, vol. 59, pp. 493 – 502, 2015.

[48] The IMBIE Team, "Mass balance of the Greenland Ice Sheet from 1992 to 2018," *Nature*, pp. 233 – 239, 2020.

[49] O. Ronneberger, P. Fischer, and T. Brox, "U-Net: Convolutional Networks for Biomedical Image Segmentation," *In: Navab N., Hornegger J., Wells W., Frangi A. (eds) Medical Image Computing and Computer-Assisted Intervention – MICCAI 2015.*, vol. 9351, pp. 234–241, 2015.

[50] D. P. Kingma and J. Ba, "Adam: A Method for Stochastic Optimization," 2014, arXiv preprint arXiv:1412.6980.

[51] M. Abadi, A. Agarwal, P. Barham, E. Brevdo, Z. Chen, C. Citro, G. S. Corrado, A. Davis, J. Dean, M. Devin, S. Ghemawat, I. Goodfellow, A. Harp, G. Irving, M. Isard, Y. Jia, R. Jozefowicz, L. Kaiser, M. Kudlur, J. Levenberg, D. Mané, R. Monga, S. Moore, D. Murray, C. Olah, M. Schuster, J. Shlens, B. Steiner, I. Sutskever, K. Talwar, P. Tucker, V. Vanhoucke, V. Vasudevan, F. Viégas, O. Vinyals, P. Warden, M. Wattenberg, M. Wicke, Y. Yu, and X. Zheng, "TensorFlow: Large-scale machine learning on heterogeneous systems," 2015, software available from tensorflow.org. [Online]. Available: https://www.tensorflow.org/

[52] GDAL/OGR contributors, *GDAL/OGR Geospatial Data*

Abstraction software Library, Open Source Geospatial Foundation, 2020. [Online]. Available: https://gdal.org

[53] L. Breiman, "Random Forests," *Machine Learning*, vol. 45, pp. 5 – 32, 2001.

[54] C. Strobl, A.-L. Boulesteix, A. Zeileis, and T. Hothorn, "Bias in random forest variable importance measures: Illustrations, sources and a solution," *BMC Bioinformatics*, vol. 8, p. 25, 2007.

[55] K. J. Archer and R. V. Kimes, "Empirical characterization of random forest variable importance measures," *Computational Statistics & Data Analysis*, vol. 52, no. 4, pp. 2249 – 2260, 2008.

[56] K. K. Nicodemus, J. D. Malley, C. Strobl, and A. Ziegler, "The behaviour of random forest permutation-based variable importance measures under predictor correlation," *BMC Bioinformatics*, vol. 11, p. 110, 2010.

[57] G. Hooker and L. Mentch, "Please Stop Permuting Features: An Explanation and Alternatives," *arXiv no. 1905.03151*, 2019.

[58] J. Lei, M. G'Sell, A. Rinaldo, R. J. Tibshirani, and L. Wasserman, "Distribution-Free Predictive Inference for Regression," *Journal of the American Statistical Association*, vol. 113, no. 523, pp. 1094 – 1111, 2018.

Martin Horwath received the diploma degree in Mathematics and the PhD degree (Dr.-Ing.) in Geodesy from Technische Universität Dresden (TU Dresden), Germany, in 1998 and 2007, respectively. He worked as a research assistant at TU Dresden from 1998 to 2008, as a postdoctoral researcher at CNES/GRGS (Centre National d'Etudes Spatiales / Groupe de Recherche de Géodésie Spatiale) and LEGOS (Laboratoire d'Études en Géophysique et Océanographie Spatiales) in Toulouse, France, from 2008 to 2010, and as a research scientist at Technical University of Munich, Germany, from 2010 to 2014. Since 2014 he has been professor holding the Chair of Geodetic Earth System Research at TU Dresden.

His research interests include applications of satellite geodesy and physical geodesy to Earth system research. A research focus is on questions of ice sheet dynamics and mass balance and the interactions between ice mass changes, solid-earth deformations and sea level change, tackled by the combination of geodetic measurements from (by satellites and in-situ) with physical modeling.

Konrad Heidler (Student Member, IEEE) received the bachelor's degree in Mathematics and the master's degree in Mathematics in Data Science from Technical University of Munich (TUM), Munich, Germany, in 2017, and 2020, respectively. He is pursuing a doctorate with the German Aerospace Center (DLR), Wessling, Germany and TUM.

His main research interests are remote sensing, computer vision, and mathematical foundations of machine learning. His current research work focuses on the application of deep learning in polar regions.

Erik Loebel received the bachelor's degree in Geodesy and Geoinformation and the master's degree in Geodesy from Technische Universität Dresden (TU Dresden), Germany, in 2016, and 2019, respectively. Since 2020, he is pursuing a PhD degree at the Chair of Geodetic Earth System Research, TU Dresden.

His research interests include remote sensing and earth observation, machine learning, signal processing and time series analysis, with a special focus on the cryosphere and polar regions. His current research aims at developing and applying deep learning methods for monitoring glacier changes in Greenland.

Julia Christmann received the diploma degree in Mathematics and the PhD degree in Applied Mechanics from Technical University of Kaiserslautern (TU Kaiserslautern), Germany, in 2010 and 2017, respectively. From 2017 to 2022, she worked as a postdoctoral researcher at Alfred-Wegener-Institut, Helmholtz Zentrum für Polar- und Meeresforschung, Bremerhaven, Germany. Since 2022, she has a professorship for Engineering at the IU International University of Applied Sciences, Erfurt, Germany.

Her research interests include glaciology and material science. A special focus lies on viscoelastic modeling and calving at Greenland and Antarctic glaciers. Her current research focuses on the inclusion of calving front positions detected by AI into the Ice sheet and Sea-level System Model (ISSM).

Mirko Scheinert is Senior Scientist at the chair of Geodetic Earth System Research, Technische Universität Dresden (TU Dresden), Germany. He completed his PhD on Orbit Dynamics of Low-Flying Satellites at the University of Stuttgart, Germany. He contributes graduate lectures in Geodesy and is active in the supervision of PhD students.

His research focuses on the determination of solid Earth deformation by geodetic methods (GNSS, gravimetry), gravity field analysis and geoid determination, the application of airborne methods in geodesy and on geodetic Earth system research. For more than 25 years his has been active in polar research, among others conducting in-situ measurements in Antarctica, Greenland and Patagonia.

Long Duc Phan graduated from the University of Dortmund and received a Diploma in informatics in 2013. He is currently working as a Software Engineer in the workgroup Remote Sensing and Modelling at the Luxembourg Insitute of Science and Technology (LIST), Luxembourg.

Previously he worked as a Data Scientist, IT Consultant, Software Developer and Scientific Programmer at different companies, organizations and public institutions like the Alfred-Wegener-Institut Helmholtz Zentrum für Polar- und Meeresforschung, Bremerhaven, Germany, and the Forschungszentrum Jülich, Jülich, Germany. His research interests are Data Science, machine learning, graphics processing units and Cloud-based services.

Angelika Humbert received her diploma in physics from the Technical University of Darmstadt, Germany, in 1996. After maternity leave she switched here research field to glaciology and completed in 2006 her doctoral thesis in ice sheet modelling at the Technical University of Darmstadt. She moved to the WWU Münster in 2008 and got later appointed in 2010 at the University of Hamburg as a professor for glaciology. In 2012 she joined the Alfred-Wegener-Institut Helmholtz Zentrum für Polar- und Meeresforschung, where she currently leads the group of ice sheet modelling and satellite remote sensing in the Section Glaciology. She is professor for ice sheet modelling at the University of Bremen and is a guest lecture at the Technical University of Darmstadt.

Her research focuses on the dynamics of ice sheets, glaciers, and ice shelves, including system studies as well as process studies. She conducts multi-scale hybrid-physics modelling of the dynamics of the Antarctic and Greenland ice sheet, projections of their sea level contribution, ice-ocean interaction, subglacial hydrology, ice fracture mechanics and viscoelastic modelling. Her second research field is satellite radar remote sensing of ice, including altimetry, SAR and polarimetry of ice. She leads airborne and field expeditions retrieving data that is used in interdisciplinary studies combining glaciological modeling, field observations and remote sensing to understands processes of ice mechanics.

Xiao Xiang Zhu (S'10–M'12–SM'14–F'21) received the Master (M.Sc.) degree, her doctor of engineering (Dr.-Ing.) degree and her "Habilitation" in the field of signal processing from Technical University of Munich (TUM), Munich, Germany, in 2008, 2011 and 2013, respectively.

She is the Chair Professor for Data Science in Earth Observation at Technical University of Munich (TUM) and the Head of the Department "EO Data Science" at the Remote Sensing Technology Institute, German Aerospace Center (DLR). Since 2019, Zhu is a co-coordinator of the Munich Data Science Research School (www.mu-ds.de). Since 2019 She also heads the Helmholtz Artificial Intelligence – Research Field "Aeronautics, Space and Transport". Since May 2020, she is the PI and director of the international future AI lab "AI4EO – Artificial Intelligence for Earth Observation: Reasoning, Uncertainties, Ethics and Beyond", Munich, Germany. Since October 2020, she also serves as a co-director of the Munich Data Science Institute (MDSI), TUM. Prof. Zhu was a guest scientist or visiting professor at the Italian National Research Council (CNR-IREA), Naples, Italy, Fudan University, Shanghai, China, the University of Tokyo, Tokyo, Japan and University of California, Los Angeles, United States in 2009, 2014, 2015 and 2016, respectively. She is currently a visiting AI professor at ESA's Phi-lab. Her main research interests are remote sensing and Earth observation, signal processing, machine learning and data science, with their applications in tackling societal grand challenges, e.g. Global Urbanization, UN's SDGs and Climate Change.

Dr. Zhu is a member of young academy (Junge Akademie/Junges Kolleg) at the Berlin-Brandenburg Academy of Sciences and Humanities and the German National Academy of Sciences Leopoldina and the Bavarian Academy of Sciences and Humanities. She serves in the scientific advisory board in several research organizations, among others the German Research Center for Geosciences (GFZ) and Potsdam Institute for Climate Impact Research (PIK). She is an associate Editor of IEEE Transactions on Geoscience and Remote Sensing and serves as the area editor responsible for special issues of IEEE Signal Processing Magazine. She is a Fellow of IEEE.